Available online at www.sciencedirect.com

ScienceDirect

www.elsevier.com/locate/brainres

Research Report

PAT4 is abundantly expressed in excitatory and inhibitory neurons as well as epithelial cells

*Sahar Roshanbin, Sofie V. Hellsten, Atieh Tafreshiha, Yinan Zhu, Amanda Raine, Robert Fredriksson**

Department of Neuroscience, Functional Pharmacology, Uppsala University, Uppsala, SE 75124, Sweden

ARTICLE INFO

Article history:
Accepted 5 February 2014
Available online 14 February 2014

Keywords:
PAT4
Amino acid transporter
Lysosomal transporter
SLC36
SLC36A4
Brain
In situ hybridization
Immunohistochemistry
Immunoflourescence
Mouse

ABSTRACT

PAT4, the fourth member of the SLC36/proton dependent amino acid transporter (PAT) family, is a high-affinity, low capacity electroneutral transporter of neutral amino acids like proline and tryptophan. It has also been associated with the function of mTORC1, a complex in the mammalian target of rapamycin (mTOR) pathway. We performed *in situ* hybridization and immunohistological analysis to determine the expression profile of PAT4, as well as an RT-PCR study on tissue from mice exposed to leucine. We performed a phylogenetic analysis to determine the evolutionary origin of PAT4. The *in situ* hybridization and the immunohistochemistry on mouse brain sections and hypothalamic cells showed abundant PAT4 expression in the mouse brain intracellularly in both inhibitory and excitatory neurons, partially co-localizing with lysosomal markers and epithelial cells lining the ventricles. Its location in epithelial cells around the ventricles indicates a transport of substrates across the blood brain barrier. Phylogenetic analysis showed that PAT4 belongs to an evolutionary old family most likely predating animals, and PAT4 is the oldest member of that family.

1. Introduction

The SLC superfamily is the largest group of transporters and currently consists of 384 members (Sreedharan et al., 2011) divided into 52 families (Hediger et al., 2013) with members belonging to the same family sharing at least 20–25% sequence homology (Hediger et al., 2004). The range of solutes transported by these proteins is exceptionally broad, including nucleotides, neurotransmitters, oligopeptides, drugs and amino acids and yet close to 40% of all SLCs are still orphan (Fredriksson et al., 2008). Of the 52 families, 11 families include amino acid transporters (Broer and Palacin, 2011; Fredriksson et al., 2008). The mammalian SLC superfamily can be divided into 4 different groups based on their evolutionary origin; α, β, γ, δ. The β-group is the second largest group and consists of SLC32, 36 and 38-families and contains the highest number of amino acid transporters sharing a common evolutionary origin and similar substrate profile

*Corresponding author.
E-mail addresses: Sahar.Roshanbin@neuro.uu.se (S. Roshanbin), Sofie.Hellsten@neuro.uu.se (S.V. Hellsten), atieh.tafreshiha@gmail.com (A. Tafreshiha), zhuyinan0108@gmail.com (Y. Zhu), Amanda.raine@medsci.uu.se (A. Raine), Robert.Fredriksson@neuro.uu.se (R. Fredriksson).

http://dx.doi.org/10.1016/j.brainres.2014.02.014
0006-8993

(Fredriksson et al., 2008; Gasnier, 2004; Sundberg et al., 2008). It is an evolutionary old group, proposed to be homologous with the ATF-group in plants (Su et al., 2004; Sundberg et al., 2008). Facilitated transporters and ion-coupled secondary active transporters constitute the SLC superfamily. The coupling of ions allows for transport against solute concentration gradients, whilst taking advantage of the electrochemical gradients. In prokaryotes and lower eukaryotes, H^+ has been the primary driving force of ion-coupled transport, whereas the vast majority of transporters in higher eukaryotes exhibit Na^+-coupling or ion-independence (Saier, 2000).

The SLC36 family consists of four members, PAT1-4, of which PAT1 and PAT2 are more widely characterized. The first member in the SLC36 family was cloned from cDNA from rat brain in 2001 (Sagne et al., 2001), characterized as the first rheogenic neuronal lysosomal amino acid transporter and named LYAAT1. It is localized to GABAergic and glutamatergic neurons in mice as well as murine axonal exocysts (Wreden et al., 2003). This suggested that members from the SLC36 family could have an important physiological role in the brain as most other transporters thus far discovered had been localized to plasma membranes or mitochondria (Palacin et al., 1998). Upon its identification, it was classified as belonging to one of the three subfamilies within the amino acid/auxin permease (AAAP) family, the other two being the VGAT transporter group, designated the SLC32 family in the SLC nomenclature (McIntire et al., 1997; Sagne et al., 1997) and the system A/N transporter group (Saier, 2000; Young et al., 1999), also known as the SLC38 family (Mackenzie and Erickson, 2004). The AAAP family was later shown to be a phylogenetically related and named the β-group in the SLC classification (Wipf et al., 2002; Young et al., 1999). The most common name for this transporter is however PAT1, as the identification at a molecular level revealed that it was a proton dependent amino acid transporter. A table of the nomenclature used for the proteins in the SLC36-family can be found in a recent review by Thwaites and Anderson (Thwaites and Anderson, 2011); in this article, we will use the PAT-nomenclature. PAT1 has a wide substrate profile including small, unbranched zwitterionic α-, β-, and γ-amino and imino acids and amino acid derivatives like GABA (Abbot et al., 2006; Anderson et al., 2004; Boll et al., 2002; Boll et al., 2003a; Chen et al., 2003a; Sagne et al., 2001) and is ubiquitously expressed but most predominantly in brain, intestine and kidney. The closely related PAT2 was cloned from mouse in 2002 (Boll et al., 2002) and has a narrower substrate profile and expression pattern. It is localized in lung, heart, testis, muscle, kidney, spleen, bone and adipose tissue (Bermingham and Pennington, 2004; Boll et al., 2002; Sundberg et al., 2008) as well as in differentiating Schwann cells (Bermingham et al., 2002). It mainly transports glycine, alanine and proline, but with a higher affinity for α-amino acids than PAT1. Mutations in the gene encoding PAT2 has also been connected to imunoglycinuria, a recessive autosomal disease affecting renal transport (Broer et al., 2008). PAT1 and PAT2 share a similar transport mechanism; both use an independently established electrochemical gradient of H^+ to drive substrate translocation and both are bidirectional (Rubio-Aliaga et al., 2004) as well as exhibiting an ordered binding profile wherein the proton is bound before the substrate. PAT2 however shows a higher proton-affinity than PAT1, and its substrate affinity is more dependent on pH (Foltz et al., 2004b). The SLC36 family also contains two additional transporters, SLC36A3 (PAT3) and SLC36A4 (PAT4). PAT3 is an orphan transporter only found in testis. The tissue localization of SLC36A3 is known on the mRNA level (Boll et al., 2003b, 2004), however no protein localization data is available. PAT4 is the most recently characterized amino acid transporter in the SLC36-family. It was first identified as LYAAT-2, in concordance with the then prescribed nomenclature (Wreden et al., 2003) and was identified on the basis of sequence similarity (Boll et al., 2002; Foltz et al., 2004b). It is ubiquitously expressed in various tissues, (Foltz et al., 2004b; Nishimura and Naito, 2005; Sundberg et al., 2008) as well as in several cancer cell lines (Heublein et al., 2010), although its detailed expression pattern has not been established. The genes coding for the human PAT1, PAT2 and PAT3 are located on chromosome 5q33.1 in rather close proximity while the gene encoding PAT4 is located on chromosome 11q14.3. However, the evolutionary history and phylogenetic relationship of the SLC36 family is largely unknown.

Recent studies show that PAT4 has a very high affinity for proline followed by tryptophan, and a lower affinity for alanine and glycine, resembling the other characterized PAT-proteins (Pillai and Meredith, 2011). As both proline and tryptophan are key substrates in neurotransmitter synthesis, this suggests that PAT4 could have an important regulatory role in neuronal transmission. Further, the studies indicate that the non-acidic pH conditions at which the transport rate is at its highest, and the apparent electroneutral transport makes PAT4 a non-H^+-coupled transporter functioning through facilitated diffusion.

To investigate the role of PAT4 in the nervous system, we have herein investigated localization and expression of the transporter in the mouse brain on mRNA- and protein level. We have shown that *Slc36a4* mRNA is widely expressed and that the protein is found mainly on the soma of neurons. We found interesting expression in the epithelial cells lining the ventricles, suggesting that PAT4 could be important in regulating transport of amino acids into the brain. A qPCR study with tissue from mice receiving the satiety-inducing amino acid leucine showed an upregulation of the mRNA expression in the paraventricular nucleus of the hypothalamus. From a phylogenetic analysis involving nine different species we conclude that PAT4 is the evolutionary oldest protein in the SLC36 family and that PAT1, PAT2 and PAT3 originated from a common ancestor after the origin of amphibians. PAT4 could therefore have retained the most original PAT function.

2. Results

Widespread Slc36a4 mRNA expression in mouse brain – Non-radioactive *in situ* hybridization was used to map the tissue expression of *Slc36a4* mRNA. Floating 70 μm coronal sections from mouse brain were hybridized with 1 μg digoxigenin labeled probe against *Slc36a4* mRNA. The mRNA expression was widespread as seen in the overview panel with annotations in Fig. 1. Marked expression was found in piriform cortex (Fig. 1G), hippocampus with particular strong

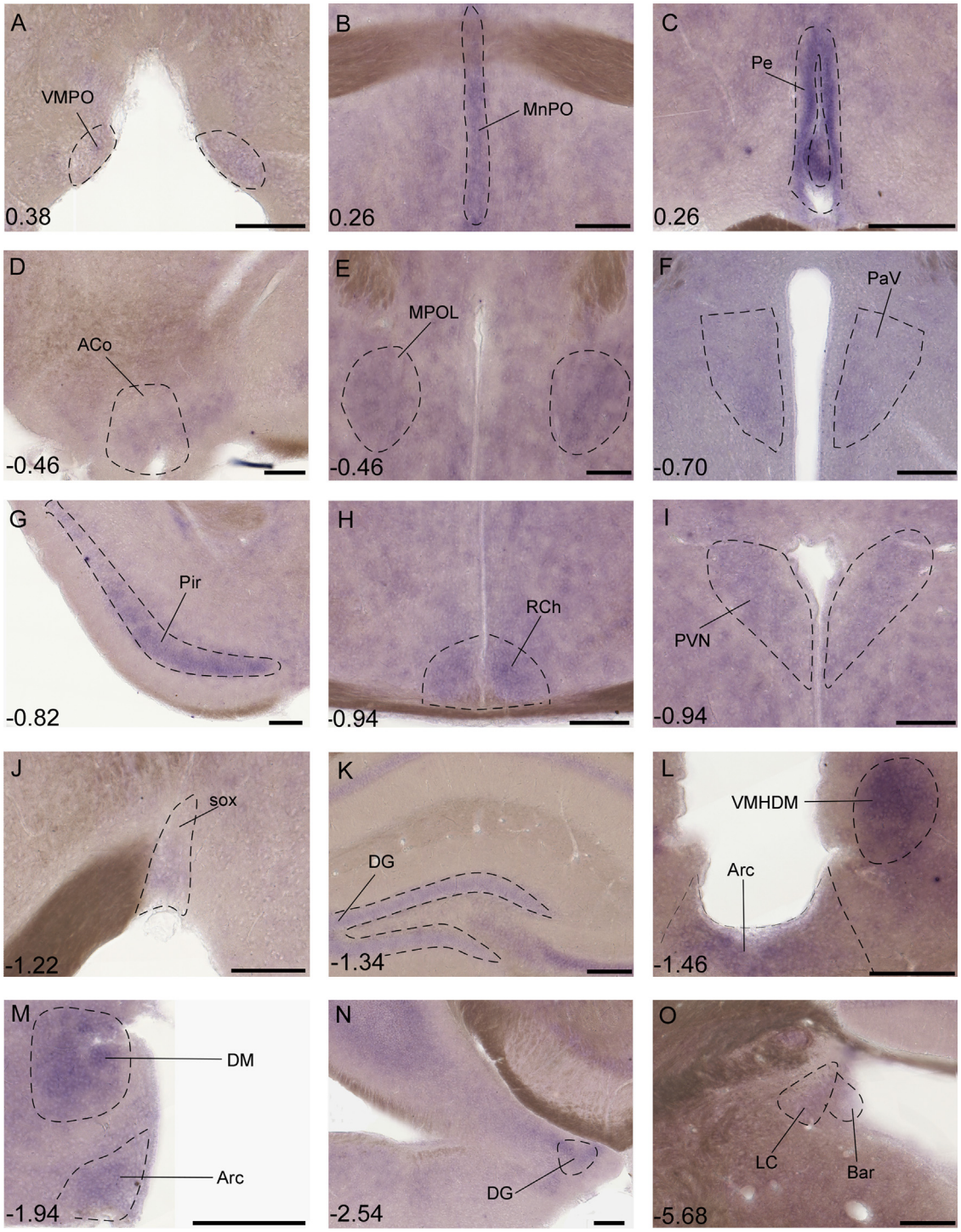

Fig. 1 – Detailed *Slc36a4* mRNA expression in 70 μm coronal WT mouse brain sections. Non-radioactive *in situ* hybridization was used for detection of *Slc36a4* mRNA using 1 μg digoxigenin-labeled anti-*Slc36A4* riboprobe. Expression was seen in piriform cortex, hippocampus and hypothalamus, in particular in ventromedial preoptic nucleus (VMPO); A, median preoptic nucleus (MnPO); B, periventricular nucleus (Pe); C, anterior cortical amygdaloid area (ACo); D, medial preoptic nucleus lateral part (MPOL); E, paraventricular nucleus of the hypothalamus, ventromedial part (PaV); F, piriform cortex (Pir); G, retrochiasmatic area (RCh); H, paraventricular nucleus (PVN); I, supraoptic nucleus (SO); J, granular layer of the dentate gyrus (GrDG); K and N, ventromedial hypothalamic nucleus, dorsomedial part (VMHDM); L, arcuate nucleus (Arc); L and M, dorsomedial hypothalamic nucleus (DM); M, locus coeruleus (LC) and Barrington's nucleus (Bar); O, Bregma coordinates and abbreviations as referenced by Franklin and Paxinos (2007).

expression in the granular layer of the dentate gyrus as well as hippocampal pyramidal cells (Fig. 1K and N). In the hypothalamus, staining was revealed in the arcuate nucleus (Fig. 1L and M), periventricular nucleus (Fig. 1C), paraventricular nucleus (Fig. 1F and I), ventromedial hypothalamic nucleus (Fig. 1L), dorsomedial hypothalamic nucleus (Fig. 1M) and in the retrochiasmatic area (Fig. 1H). Furthermore, *Slc36a4* mRNA was detected in the supraoptic nucleus (Fig. 1J), lateral part of medial preoptic nucleus (Fig. 1E), ventromedial preoptic nucleus (Fig. 1A), medial preoptic nucleus lateral part (Fig. 1B), cortical amygdaloid area (Fig. 1D) as well as locus coeruleus and Barrington's nucleus (Fig. 1O).

Verifying the specificity of the PAT4 antibody – Combined *in situ* hybridization and immunohistochemistry was used to investigate co-localization of *Slc36a4* mRNA with the PAT4 protein to verify the specificity of the antibody, along with a Western Blot analysis, both shown in Fig. 2. The *in situ* hybridization was performed using the riboprobe mentioned previously and the fluorescent immunohistochemistry using a monospecific polyclonal anti-PAT4 antibody with a recombinant epitope signature tag, PrEST. The Western Blot analysis showed a single band approximately at 65–70 kDA, slightly larger than the predicted protein size of 56.2 kDa (Fig. 2A). This larger size could be due to posttranslational modifications; this is highly possible as the sequence contains five strong N-glycosylation sites, as predicted by the NetNGlyc server (http://www.cbs.dtu.dk/services/NetNGlyc/). In addi tion, the combined *in situ* hybridization and immunohisto chemistry revealed an overlap between the mRNA and the PAT4-protein, thus further verifying the specificity of the antibody (Fig. 2B).

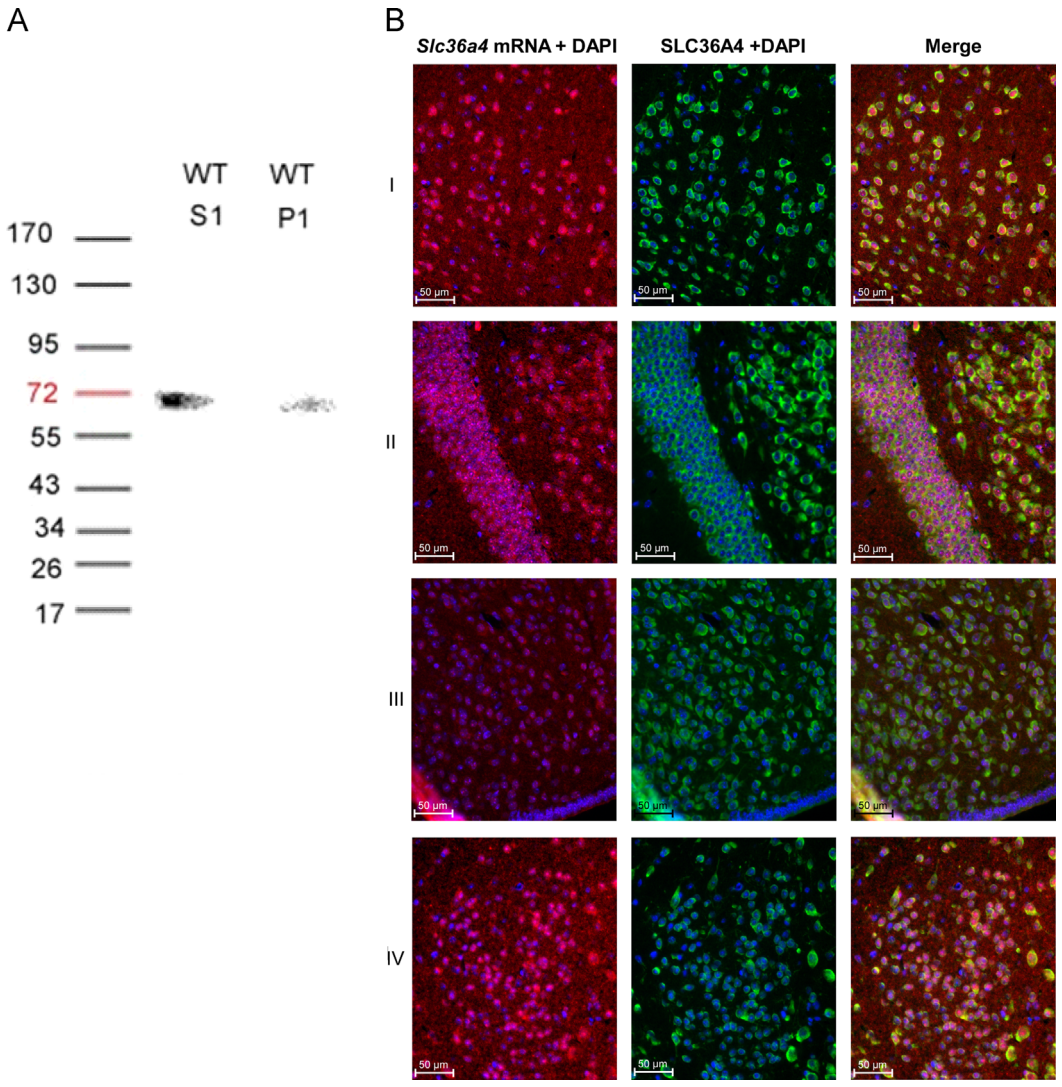

Fig. 2 – Western Blot and combined *in situ* hybridization and immunohistochemistry. (A) Western Blot on fractionated WT mouse brain revealed a strong band at approximately 65–70 kDa in the S1 fraction and a weaker band of the same size in the P1 fraction. For definition of S1 and P1, see Section 4. The combined *in situ* hybridization and immunohistochemistry (B) showed an overlap, here seen in (I) retrosplenial dysgranular cortex (RSD), (II) granular and molecular layer of the dentate gyrus (GrDG and MoDG, respectively), (III) medial posterior and lateroposterior part of the arcuate nucleus (ArcMP and ArcLP, respectively) and (IV) posteriomedial cortical nucleus of the hypothalamus (PMCo). Abbreviations as referenced to by Franklin and Paxinos (2007).

PAT4 is expressed in neurons and epithelial cells – Double immunohistochemistry with fluorescent markers on WT paraffin sections was used for determination of cell-specific expression of PAT4. A high degree of co-localization of PAT4 with the neuronal marker NeuN (Mullen et al., 1992) was found in cortex, indicating expression of PAT4 on the

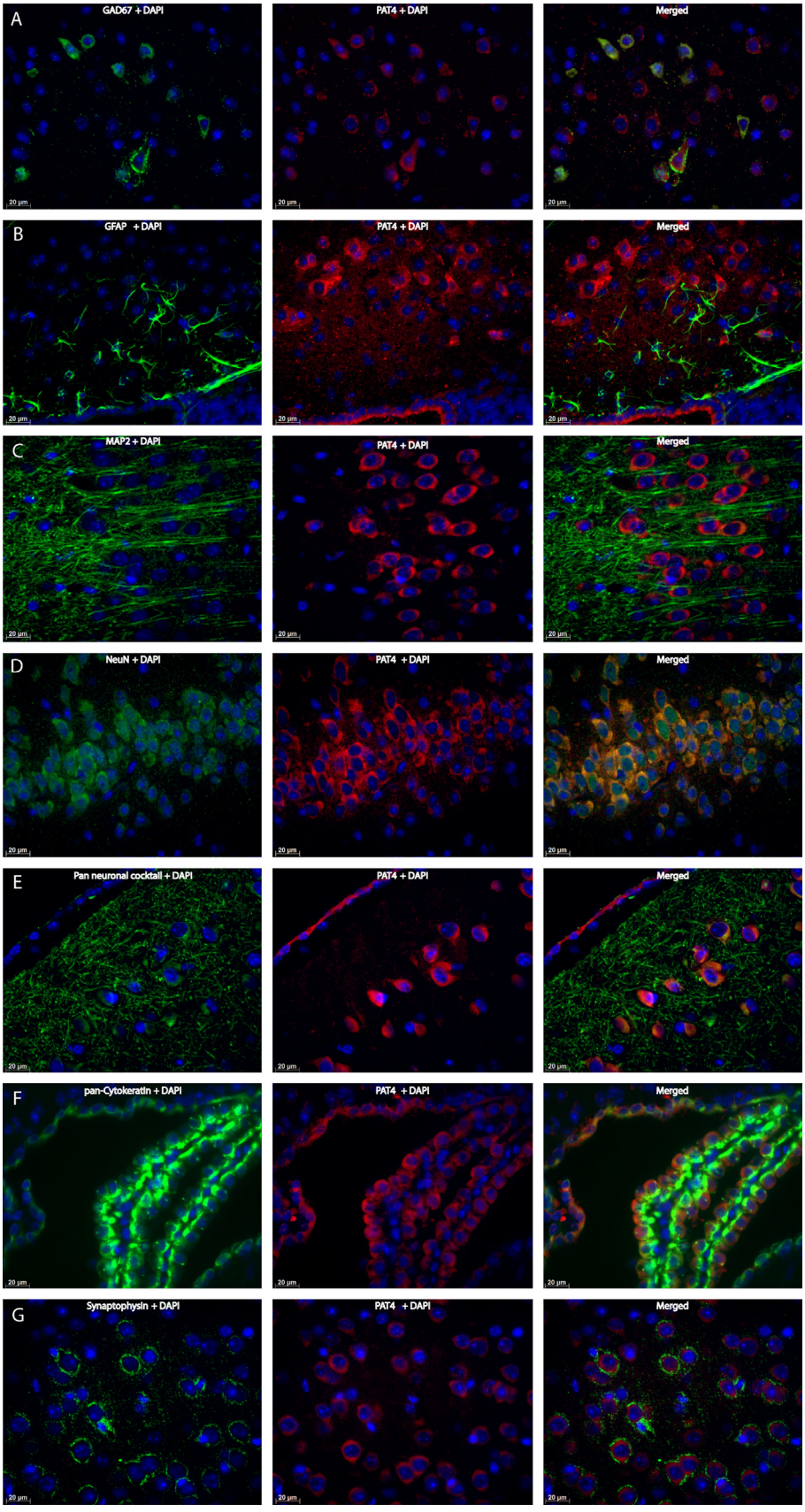

somatodendritic part of both excitatory and inhibitory neurons (Fig. 3D). The latter was also confirmed through co-staining with glutamic acid decarboxylase 67 protein (GAD67), a marker for inhibitory GABAergic neurons (Kaufman et al., 1991) showing a co-expression of PAT4 and GAD67 in some but not all PAT4-expressing cells in cortex (Fig. 3A). We observed no overlap between PAT4 and MAP2, a marker for neuronal microtubule-associated protein 2 (Bernhardt and Matus, 1984), suggesting that PAT4 is not found in neuronal axons (Fig. 3C). Staining with the whole-neuron marker specific to axons, dendrites, nuclei and soma of neurons, the Pan neuronal cocktail (Doyle et al., 2010) (Fig. 3E) and PAT4 also shows expression of PAT4 mainly in neuronal cell bodies. Overlap with the two aforementioned markers indicates that PAT4 is predominantly expressed in the soma, with no overlapping expression in neuronal fibers. There was no co-expression of PAT4 and synaptophysin (Fig. 3G), a marker of pre-synaptic vesicles (Wiedenmann and Franke, 1985) suggesting that PAT4 is not present at synapses. There was no overlap in expression between PAT4 and the astrocytic marker glial fibrillary acidic protein (GFAP) (Reeves et al., 1989) (Fig. 3B); however, there was a high degree of overlap between PAT4 and pan-Cytokeratin, an epithelial marker (von Overbeck et al., 1985), around the lateral ventricles (Fig. 3F), showing expression of PAT4 in epithelial cells.

PAT4 displays intracellular expression – Triple immunohistochemistry on immortalized hypothalamic cells was performed to study the subcellular localization of PAT4, using the PAT4-antibody along with the membrane marker WGA and the lysosomal markers Cathepsin-D and LAMP2, respectively. The lack of co-localization of PAT4 and WGA suggests that PAT4 is not expressed on the plasma membrane but rather intracellularly, seen in Fig. 4A and C. The channel intensities along the white arrows in Fig. 4A and C are depicted in the adjacent graphs, respectively (Fig. 4B and D), showing that peaks from the WGA staining do not co-localize with peaks from the PAT4- and the lysosomal staining, suggesting that PAT4 is expressed intracellularly. The staining in the images along with the graphs also show a partial co-localization of PAT4 and the lysosomal markers LAMP2 and Cathepsin-D.

High PAT4 expression in hippocampus, hypothalamus and piriform cortex – The expression of PAT4 in 70 μm coronal sections of mouse brain was investigated through immunohistochemistry with DAB, using the PAT4-antibody, as shown in Fig. 5. The expression pattern follows that of the *in situ* hybridization with a high degree of staining in the pyramidal cells (Pyr) and the molecular and granular layers of the dentate gyrus in the hippocampus (PoDG and GrDG, respectively) (Fig. 5E), in the arcuate nucleus (Arc) and the dorsomedial hypothalamic nucleus (DMH) (Fig. 5D) and piriform cortex (Fig. 5C). High levels of expression are also found in the suprachiasmatic nucleus (SCh) and the horizontal limb of the diagonal band (HDB), the periventricular nucleus (Pe), the bed nucleus of the stria terminalis (STMPI) (Fig. 5A) as well as in the retrochiasmatic area (RCh). Other areas with interesting staining in the hypothalamus include; ventromedial hypothalamic nucleus (VMH) and the peduncular part of lateral hypothalamus (PLH) (Fig. 5B). Further, strong staining is seen in the basomedial amygdala (BMA) and the central amygdaloid nucleus (Ce). The lateral division of the mamillary nucleus (ML), substantia nigra (SN), ventral tegmental area (VTA) and the interfascicular nucleus (IF) (Fig. 5F) also exhibited strong staining, accompanied by the medial accessory oculomotor nucleus (MA3) and the interpeduncular nucleus rostral subnucleus (IPR).

PAT4 is the evolutionary oldest member of the SLC36-family – To investigate the evolutionary history of the SLC36 family we constructed a phylogenetic tree based on all SLC36 like sequences from nine different species (Fig. 6A). We also included the complete set of SLC32 and SLC38 family proteins from human. Here we show that the SLC36, SLC32 and SLC38 sequences form three separate basal branches in the phylogeny. The analysis also suggests that there was a single SLC36 gene before the split of *Trichoplax adhaerens* and that this gene was duplicated before the teleost fish lineage. Interestingly, the PAT1, 2 and 3 were formed from a common ancestor after the split of amphibians. PAT1, 2 and 3 are located on chromosome 5q33.1 next to each other, covering a genomic are of less than 250,000 bases. Also these genes have highly similar exon–intron organization, all consisting of 10–11 coding exons which taken together suggests that they were formed by a recent local duplication of genomic material. We propose an evolutionary scheme for how the SLC36 family was formed (Fig. 6B).

Fig. 3 – Cellular localization of PAT4 to neurons and epithelial cells – Double immunohistochemistry with fluorescent markers on WT paraffin sections was used to determine the cellular localization of PAT4. PAT 4 was stained in red using the monospecific polyclonal PAT4 antibody, and all markers used were stained in green. The cell nuclei have been stained with DAPI, seen in blue. (A) Co-localization with GAD67; most neurons stained with GAD67, a GABAergic marker for most inhibitory neurons are also stained with PAT4 in cortex, but not the other way around. This indicates that PAT4 is expressed in both inhibitory and excitatory neurons. (B) Co-localization with GFAP; there is no overlap between PAT4 and the astrocytic marker GFAP in cortex. (C) Co-localization with MAP2; the overlapping expression of the neuronal microtubule marker MAP2 and PAT4 in cortex in the merged image indicates an expression of PAT4 in the neuronal soma. (D) Co-localization with NeuN; the merged image shows a high degree of co-localization of PAT4 and the neuronal marker NeuN in cortex, indicating that PAT4 is expressed in most neurons, both inhibitory and excitatory. (E) Co-localization with Pan neuronal cocktail; the co-expression of PAT4 in cortex with the whole neuron marker Pan neuronal cocktail aimed at axons, dendrites, nuclei and soma of neurons indicate that PAT4 is expression is confined to the neuronal soma. (F) Co-localization with pan-Cytokeratin; the merged image depicting he overlap between PAT4 and the epithelial marker pan-Cytokeratin around the lateral ventricle suggests that PAT4 is expressed in epithelia. (G) Co-localization with synaptophysin; there is no overlap between PAT4 and synaptophysin, a marker for pre-synaptic vesicles.

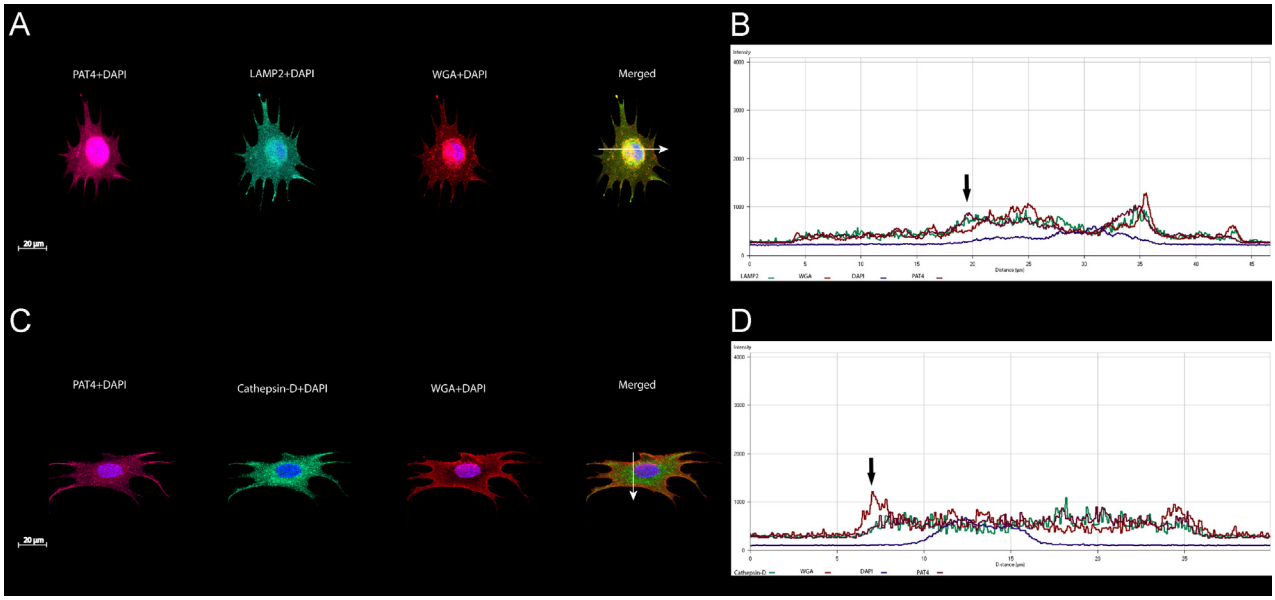

Fig. 4 – Intracellular localization of PAT4. Triple immunohistochemistry with fluorescent markers on hypothalamic cells was used to investigate the subcellular localization of PAT4 as well as the overlap with the lysosomal markers LAMP2 and Cathepsin D. Confocal images of the cells were analyzed using the LSM 510 software, with the channel intensities along the arrows in the merged images depicted in the graphs. PAT4 was stained in violet, WGA in red, DAPI in blue and the markers LAMP2 and Cathepsin-D in green. The confocal images of the immunohistochemistry show a partial co-localization of PAT4 and LAMP2 (A) and Cathepsin-D (B) and the respective graphs showing the different channel intensities show no co-localization between PAT4 and WGA, the membrane marker (see arrows in the graphs).

3. Discussion

We have previously shown that PAT4 is expressed in many tissues in rat using quantitative realtime PCR (Sundberg et al., 2008). Here, we show using *in situ* hybridization that *Slc36a4* mRNA is abundantly expressed also in mouse brain, predominantly in piriform cortex, hippocampus and hypothalamus. We also performed the first immunohistological analysis of PAT4 showing a high abundance in mouse brain similar to the mRNA expression. We used fluorescent double immunohistochemistry to show that PAT4 is localized mainly in the soma of both inhibitory and excitatory neurons, but not in any astrocytes or glia cells. Fluorescent triple immunohistocheimstry on hypothalamic cells show an apparent intracellular localization of PAT4 with a partial overlap with lysosomal markers. The polyclonal antibody used here also shows some staining in the nucleus. It is possible that this staining is unspecific at the concentrations used as it is unlikely that an amino acid transporter has a physiological function in the nucleus. We have chosen to treat the nuclear staining with caution and do not discuss this further here. We performed a phylogenetic analysis (Fig. 6A) that showed that members from the SLC36 family were present already in the placozoan *T. adhaerens*, which is a sister group to the bilaterian group containing most animals. This shows that the SLC36 family is evolutionary old and most likely predates animals. Interestingly, PAT4 appears to be the evolutionary oldest member, and the previously studied members, PAT1, PAT2 and PAT3 originated from a common ancestral gene within the tetrapod lineage. The clustering and closer evolutionary relationship of PAT1-3 suggests that there are two subfamilies within the SLC36 family, the PAT1-3 subfamily and PAT4 subfamily. Data also suggests that these subfamilies are distinct not only in evolutionary terms, but also functionally. The two subfamilies differ in regards to expression pattern and substrate profile as well as mode of transport, making the functional characterization of PAT4 of interest. The transport mechanism exerted so far by the previous members PAT1 and PAT2 is a proton-dependent; in where an ordered binding of a proton followed by subsequent translocation of both proton and substrate across the membrane in which it is located. It has been shown that various factors can affect the transport rate and the substrate affinity, in particular pH and membrane potential to different degrees. It has also been shown that transport of certain substrates, mainly short-chain fatty acid-derivatives, by PAT1- and PAT2 is electroneutral rather than rheogenic (Foltz et al., 2004a). When the transport mechanism of PAT4 was investigated, a similar theory arose; the apparent electroneutrality of the transport taken together with the basic pH giving the best transport rate suggested that this transporter not be proton-dependent, in contrast to PAT1 and PAT2.

Substrate analysis has found proline to be the main substrate of PAT4, followed by tryptophan. Considering the interchangeable qualities of proline, glutamate and glutamine and the expression of other proline-specific transporters in rat brain in glutamatergic neuronal subpopulations, the transport of proline into these areas has been suggested to play a role in excitatory neurotransmission (Johnson and Roberts, 1984). The metabolism of proline in brain is further

accentuated by the neurological disorders that deficiencies are associated with, suggesting proline to have an important role in brain function and development. PAT1 is also known to transport proline, as well as alanine, which is also involved in excitatory neurotransmission (Westergaard et al., 1993). Although these amino acids can both be synthesized in glial cells, neither PAT1 nor PAT4 are expressed in glial cells. However, considering the expression of PAT4 in both excitatory and inhibitory neurons, the role of PAT4 in these neurons cannot be confined to glutamatergic neurotransmission. Another high-affinity substrate of PAT4 is the aromatic, essential amino acid tryptophan. Tryptophan is metabolized into serotonin, an inhibitory neurotransmitter (Hamon et al., 1979).

We show that PAT4 is mainly found on the cell bodies of neurons, with a staining pattern surrounding the cell nuclei, while PAT1 have been shown to be expressed in the lysosomes as well as in the plasma membrane (Wreden et al., 2003). This is supported also by the fact that PAT1 and PAT2 transport is dependent on the H^+ gradient, a feature common for transporters expressed in internal membranes such as lysosomes (Chen et al., 2003b) and synaptic vesicles. The overlaps of PAT4 with the epithelial cell marker pan-Cytokeratin around the ventricles in the brain indicate that PAT4 is involved in transporting substrates from the cerebrospinal fluid across the choroid plexi. This is in line with previous findings of proline and neutral amino acid transport across choroid plexus, albeit with a low affinity (Ross and Wright, 1984). The findings in the described immunolocalization studies also point to a possible differential subcellular expression of PAT4, previously exhibited by other transporters (Geerlings et al., 2002; Soontornmalai et al., 2006).

To summarize, we have performed a detailed analysis of *Slc36a4* mRNA distribution in mouse brain, and an immunohistological analysis mapping the protein expression in mouse brain, both showing an abundant expression in piriform cortex, hippocampus and hypothalamus. Fluorescent immunohistochemistry revealed intracellular localization of PAT4 in inhibitory and excitatory neurons. PAT4 is also present in epithelial cells lining the ventricles in the brain, suggesting that it is involved in transporting neutral amino acids like proline from the blood. Phylogenetic analysis shows that SLC36-family is evolutionary old, and that PAT4 is the oldest member, differing in both chromosome location and transport mechanism from the other characterized members. RT-PCR on brain tissue from mice receiving leucine in diet showed an upregulation of *Slc36a4* mRNA in the PVN, in line with the finding that leucine is an activator of mTOR, along with recent studies showing that PAT4 together with PAT1 is required for mTORC1 activation.

4. Experimental procedures

4.1. Ethics statement

Animal care procedures for C57Bl6/J adult male mice were approved by the local ethical committee in Uppsala and followed the guidelines of European Communities Council Directive (86/609/EEC).

4.2. Tissue preparation

Animal care procedures for C57Bl6/J adult male mice were approved by the local ethical committee in Uppsala and followed the guidelines of European Communities Council Directive (86/609/EEC). Adult male C57Bl6/J mice (Taconic M&B, Denmark) were intraperitoneally injected with 400 mg/kg sodium pentobarbital (APL, Sweden) and transcardially perfused with phosphate buffered saline (PBS) followed by 4% formaldehyde. (Histolab, Sweden). Immediately following the perfusion, the brains were removed and immersed in the same fixative at 4 °C overnight. The brains were then transferred to 2% formaldehyde and kept there until sectioning. Free floating tissue sections were acquired by washing the brains with PBS (2 × 5) followed by embedding in 4% agarose (Pronadisa Conda, Spain) and sectioning (70 μm) on a Leica VT1000S vibratome (Leica Microsystems, Germany). Free floating sections for immunohistochemistry were kept in PBS at 4 °C after sectioning, whereas sections for *in situ* were dehydrated with successive methanol washes and stored in 100% methanol at −20 °C. For paraffin-embedded tissue sections, the brain was fixed in zinc-formalin (Richard-Allan Scientific) for 18–24 h at 40 °C before dehydration and paraffin infusion (Tissue-Tek vacuum infiltration processor; Miles Scientific). The sections were cut (7 μm) using a Microm 355S STS cool cut microtome (Thermo Fisher Scientific, Germany) attached on Superfrost Plus slides (Menzel-Gläser, Germany), dried overnight at 37 °C, and stored at 4 °C until use.

4.3. In situ hybridization on free floating sections

Free floating sections were rehydrated by successive 10 min washes in methanol and phosphate buffered saline with 0.1% Tween-20 (Sigma–Aldrich, Sweden), PBT. The sections were then bleached in 6% hydrogen peroxide for 15 min, followed by washes in PBT before incubation in 0.5% Triton X-100 (Sigma–Aldrich, Sweden) for 5 min. After additional washes in PBT, the sections were digested with 20 μg/mL proteinase K (Invitrogen, Sweden) for 3 min and the digestion was stopped using PBT. The sections were postfixated in 4% formaldehyde (HistoLab, Sweden) for 35 min before a 2 h pre-incubation in hybridization buffer (50% formamide (Sigma–Aldrich, Sweden) 5 × SSC, 1% SDS, 50 μg/mL tRNA (Sigma–Aldrich, Sweden), 50 μg/mL heparin (Sigma–Aldrich, Sweden) in PBT) at 55 °C. The *Slc36a4* probe (1 μg/mL) diluted in hybridization buffer was heat-denatured at 80 °C for 5 min, cooled on ice and added to the sections for overnight hybridization at 55 °C. Unbound probe was washed off by sequential 3 × 30 min washes in buffer 1 (50% formamide, 2 × SSC, 0.1% Tween-20) and buffer 2 (50% formamide, 0.2 × SSC, 0.1% Tween-20) at 55 °C. The sections were washed in 0.1% Tween-20 in Tris-buffered saline (TBST) for 2 × 5 min with subsequent incubation in 1% blocking reagent (Roche Diagnostics Scandinavia, Sweden) for 2 h. The blocking was followed by incubation in the anti-digoxigenin antibody conjugated to alkaline phosphatase (Roche Diagnostics Scandinavia, Sweden)) diluted 1:5000 in blocking solution overnight at 4 °C. Unbound antibody was washed off with 5 × 10 min washes with TBST with 2 mM levamisole (Thermo Fischer Scientific, USA), followed by incubation in NTMT with 2 mM levamisole

(100 mM NaCl, 10 mM Tris HCl, pH 9.5, 50 mM $MgCl_2$, 0.1% Tween-20) for 10 min before color development with BM-Purple AP enzyme substrate (Roche Diagnostics Scandinavia, Sweden) at 37 °C. After mounting in 50% glycerol and TBST, the sections were scanned with Mirax Pannoramic Scanner (3dHistech, Hungary). For *in situ* hybridizations all solutions were made with

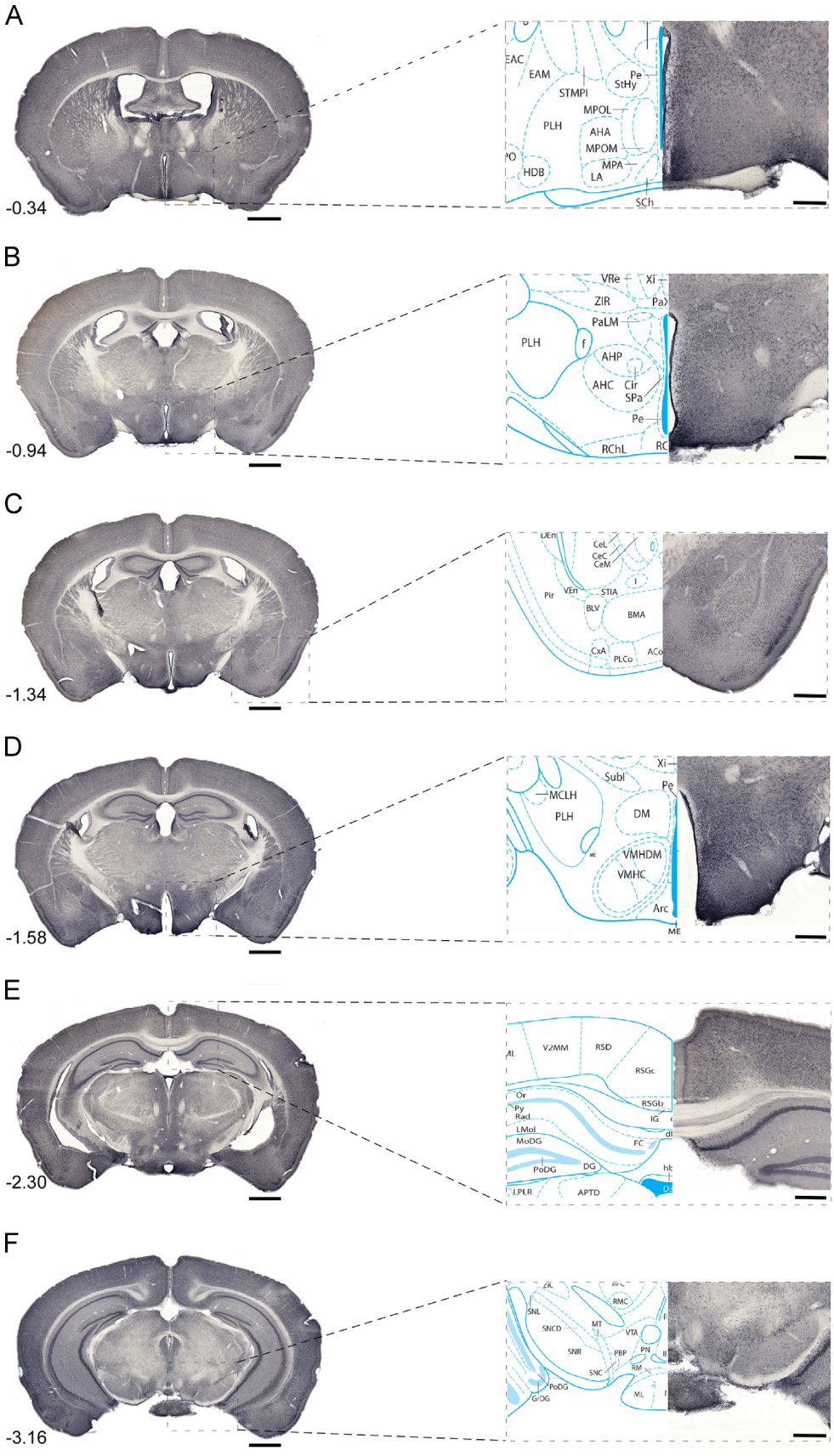

diethylpyrocarbonate (DEPC)-treated ddH_2O to ensure absence of RNAses.

4.4. Double in situ/immunohistochemistry on paraffin sections

The paraffin sections were deparaffinized in X-Solve (2 × 10 min) (Meditek histotechnik, Germany) and rehydrated through 2 min washes in graded ethanol to PBS, followed by washes in PBS (2 × 2 min). The sections were postfixated in 4% formaldehyde (Histolab, Sweden) for 10 min in room temperature and digested with proteinase K (Invitrogen, USA) for 15 min. The sections were then refixated in the same fixative for 5 min at room temperature, washed in PBS (2 × 5 min) and acetylated with 1.3% triethanolamine Sigma–Aldrich, Sweden), 0.06 HCl (Sigma–Aldrich, Sweden), 2% acetic anhydride (Fluka, Switzerland) in DEPC for 10 min. Following this, sections were treated with 1% Triton X-100 (30 min) with subsequent washes in PBS (3 × 5 min) prior to pre-hybridization in hybridization buffer 50% formamide (Sigma–Aldrich, Sweden), 5 × SSC, pH 4.5, 5 × Denhardt's, 250 μg/mL of yeast transfer RNA (Sigma–Aldrich, Sweden), sheared salmon sperm DNA (500 μg/mL Ambion) in 0.1% diethyl pyrocarbonate-treated water) for 2 h at 55 °C. The sections were then hybridized at 55 °C with heat denatured *Slc36a4* probe (0.7 μg/mL) at 55 °C overnight. Unbound probe was removed with washes in pre-warmed 5 × SSC at 55 °C, followed by incubation in 0.2 × SSC for 1 h at 55 °C, and subsequent washes in 0.2 × SSC (2 × 5 min) at room temperature. Thereafter, the sections were pre-blocked in blocking solution (0.1 M Tris HCl, pH 7.5, 0.15 M NaCl, and 10% albumin bovine serum (Sigma-Aldrich, Sweden) for 1 h. The sections were incubated in alkaline phosphatase-conjugated anti-digoxigenin Fab fragments (Roche Diagnostics Scandinavia, Sweden) diluted 1:2500 and primary antibody anti-PAT4 (1:200) in blocking solution at 4° overnight. Following the incubation, the sections were washed with TBST with 2 mM levamisole and NTMT with 2 mM levamisole as previously described. The sections were developed in Fast Red Solution (Roche Diagnostics Scandinavia, Sweden) followed by washes in PBS (3 × 5 min) and incubation in secondary donkey anti-rabbit-488 antibody (Invitrogen, Sweden) for 1 h. Following washes in PBS (3 × 5 min), the sections were incubated in the cell nucleus marker, 4′,6-diamidino-2-phenylindole (DAPI, 1:1250, Sigma–Aldrich, Sweden) diluted in blocking solution for 5 min. The sections were washed in PBS (3 × 5 min) and mounted with DTG antifade mounting medium (2.5% DABCO (Sigma–Aldrich, Sweden), 50 mM Tris, pH 8.6, 90% glycerol) and photographed using a fluorescent microscope (Zeiss Axioplan2 imaging) connected to a camera (AxioCam HRm) with the Carl Zeiss AxioVision version 4.7 software.

4.5. Fluorescent immunohistochemistry on paraffin sections

The sections were deparaffinized and rehydrated as previously described and. The sections were heated to 100 °C in 0.01 M citric acid pH 6.0 (10 min) (Sigma–Aldrich, Sweden) and then washed in PBS (3 × 5 min), placed in a humidified chamber and incubated with primary rabbit anti-PAT4 (1:200, Sigma–Aldrich, Sweden) mouse anti-NeuN (1:400, Millipore, Sweden), chicken anti-GFAP (1:400, Abcam, United Kingdom), mouse anti-MAP2 (1:500, Sigma), mouse anti-synaptophysin (1:200, BD Transduction Laboratories), mouse anti-pan-Cytokeratin (1:400, Sigma Aldrich, Sweden), mouse anti-pan neuronal marker (1:100, Millipore, Sweden), mouse anti-Gad67 (1:200, Millipore, Sweden) diluted in supermix (Tris-buffered saline, 0.25% gelatin, 0.5% Triton X-100) overnight at 4 °C. The PAT4 antibody was a rabbit polyclonal antibody raised against the sequence REELDMDVMRPLINEQNFDGTS-DEEHEQELLPVQKHYQLDDQEGISFVQTLMHLLKGNIGTGL in the human PAT4. This sequence is 85% identical in mouse PAT4 and less than 40% conserved in the other PAT family members. Unbound antibodies were washed off with PBS (3 × 5 min), followed by incubation in 1:400 diluted secondary antibodies donkey anti-rabbit-594, donkey anti-rabbit-488, goat anti-mouse-594, goat anti-mouse-488, and goat anti-chicken-488 (all Invitrogen, Sweden) in supermix for 3 h. The sections were subsequently washed in PBS (1 × 4 min) and stained with DAPI (1:1250) for 5 min prior to mounting using DTG and photographed as previously described.

4.6. Fluorescent immunohistochemistry on hypothalamic cells

Immortalized embryonic mouse hypothalamus cell line N25/2 (mHypoE-N25/2, Cellutions Biosystems Inc., Canada) was cultured for 40 h on glass slides previously coated with 10 μg/mL poly-L-lycine. Cells were rinsed with PBS before fixation in 4% paraformaldehyde (Sigma–Aldrich, Sweden) for 15 min. Slides were blocked in supermix (0.25% gelatin and 0.5% Triton X-100 in TBS) for 1 h at room temperature before incubation in primary antibodies; the fluorescently labeled membrane marker wheat germ agglutinin (WGA, 2 μg/mL,

Fig. 5 – High PAT4 expression in hippocampus, hypothalamus and piriform cortex – Immunohistochemistry with DAB was used for tissue mapping of PAT4 in 70 μm floating coronal section of WT mouse brain. (A)–(F) are overview pictures with appertaining magnified images. Strong expression was seen in (A) suprachiasmatic area (SCh), nucleus of the horizontal limb of the diagonal band (HDB), periventricular nucleus (Pe), bed nucleus of the stria terminalis (STMPI), (B) retrochiasmatic area (RCh) peduncular part of lateral hypothalamus (PLH), (C) piriform cortex (Pir), basomedial amygdala (BMA), central amygdaloid nucleus (Ce), (D) arcuate nucleus (Arc), ventromedial hypothalamic nucleus (VMH), dorsomedial hypothalamic nucleus (DMH), (E) cortex, the hippocampal pyramidal cells, fasciola cinereum (FC), granular layer of the dentate gyrus (GrDG), polymorphic dentate gyrus (PoDG), lateral division of mamillary nucleus (ML), (F) substantia nigra compact dors tier (SNCD), substantia nigra compact (SNC), substanita nigra lateral (SNL), ventral tegmental area (VTA), parabrachial pigmented nucleus of the VTA (PBP), medial accessory oculomotor nucleus (MA3), interfascicular nucleus (IF), interpeduncular nucleus rostral subnucleus (IPR). Bregma coordinates and abbreviations as referenced by Franklin and Paxinos (2007).

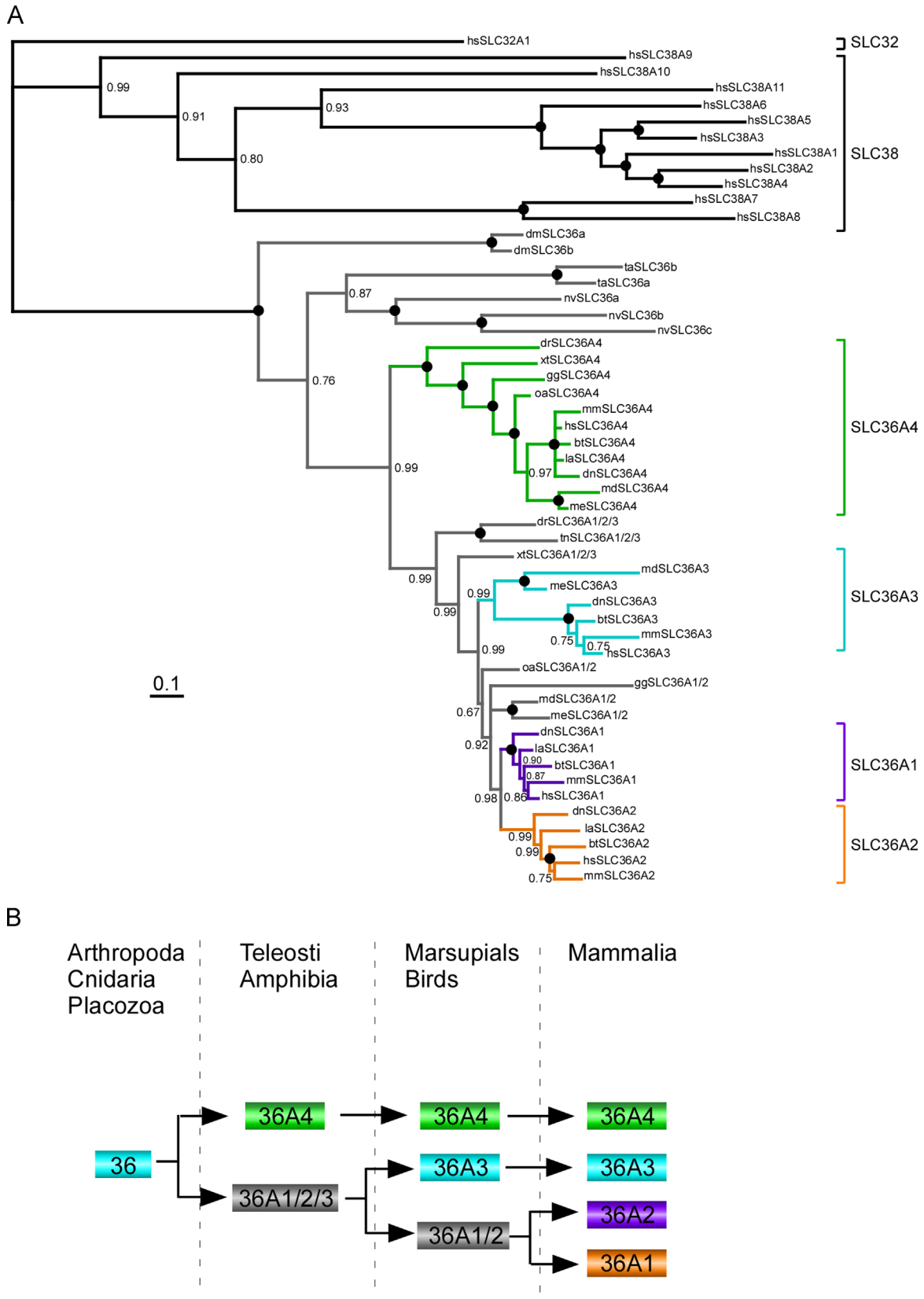

Fig. 6 – (A) Phylogenetic tree showing the evolutionary relationship between SLC32, SLC36 and SLC38 families as well as the evolutionary history of the SLC36 family. The tree was constructed using MrBayes 3.2 (Huelsenbeck and Ronquist, 2001; Ronquist and Huelsenbeck, 2003), and drawn with branchlengths representing evolutionary distance. The numbers at the nodes represents posterion probability (pp) values, all nodes with a pp value of 1.00 was marked with a black circle. The different subtypes within the SLC36 family are drawn in separate colors. Species abbreviations: md (*Monodelpih domestica*), oa (*Ornithorhynchus anatinus*), me (*Macropus eugenii*), mm (*Mus musculus*), hs (*Homo sapiens*), bt (*Bos taurus*), la (*Loxodonta africana*), tn (*Tetraodon nigroviridis*), dr (*Danio rerio*), xt (*Xenopus tropicalis*), gg (*Gallus gallus*), dn (*Dasypus novemcinctus*), dm (*Drosophila melanogaster*), ta (*Trichoplax adhaerens*), nv (*Nematostella vectensis*). (B) Proposed evolutionary scheme for how the SLC36 family was formed.

Invitrogen, Sweden) rat anti-LAMP2 (1:100, Abcam, United Kingdom), goat anti-cathepsin-D (1:100, Santa Cruz Biotechnology, Santa Cruz, CA, USA), and rabbit anti-PAT4 (1:100, Sigma Aldrich, Sweden) overnight at 4 °C. The following day, slides were rinsed in PBS 3 × 10 min, incubated in secondary antibodies diluted in supermix; goat anti-rabbit-633, goat anti-rat-488 and donkey anti-goat-488, (1:400, all Invitrogen, Sweden) for 1 h at room temperature. Slides were washed in PBS 2 × 10 min, incubated in DAPI (1:1250 in PBS) for 5 min in room temperature and rinsed 2 × 5 min before they were mounted in DTG. Images were collected on a Zeiss LSM 510 Meta confocal microscope (Carl Zeiss Inc., Thornwood, NY) and analysis of images was performed using the LSM Software.

4.7. *Non-fluorescent immunohistochemistry on free floating sections*

Free floating sections were rinsed in Tris-buffered saline (TBS) for 4 × 10 min before and after incubation in 3% hydrogen peroxide/10% methanol in TBS for 20 min. The sections were pre-blocked in 1% blocking reagent (Roche Diagnostics, Scandinavia, Sweden) diluted in TBS for an hour and thereafter incubated in rabbit anti-PAT4 (1:1500) diluted in supermix (0.25% gelatin and 0.5% Triton X-100 in TBS) overnight at 4 °C. The sections were further rinsed in TBS for 5 × 10 min and incubated in biotinylated secondary goat-anti rabbit antibody (1:400) diluted in supermix, and rinsed in TBS before incubation in avidin–biotin complex (1:800; Vectastain ABC kit, Vector Laboratories, USA) diluted in supermix. The peroxidase was visualized in black with 0.05% 3,3′-diaminobenzidine tetrahydrochloride (DAB), 0.35% NiCl and 0.01% H_2O_2 after 10 min incubation. Sections were mounted on gelatin-coated slides (Menzel-Gläser, Germany), air-dried overnight, dehydrated in ascending concentrations of ethanol, soaked in xylene, and mounted in DPX (Sigma–Aldrich, USA). The analysis was performed using a Pannoramic midi scanner as previously described.

4.8. *Western Blot*

Western Blot analysis was performed on brain tissue from one adult, male C57Bl6/J wild type mouse (Taconic M&B, Denmark). Crude protein extraction was performed by homogenizing 0.2 mg brain tissue with equal amount of glass beads in 1 mL of lysis buffer (50 mM Tris-HCl pH 8, 150 mM NaCl, 4 mM MgCl, 0.5 mM EDTA, 2% Triton X-100 and 1 mM Protease inhibitor PMSF diluted in isopropanol (Sigma–Aldrich, USA)) with a Bullet blender (Next Advance, USA). A short centrifugation was then performed and the supernatant was transferred to a new tube. Subsequently, the homogenate was centrifuged at 1000 × *g* for 10 min, receiving pellet 1 (P1) and supernatant 1 (S1), with the supernatant transferred followed by a new centrifugation at 13,000 × *g* for 15 min, receiving pellets 2 (P2) and supernatant 2 (S2). Protein concentrations were determined by protein assay DC according to manufacturer's instructions (Bio-Rad Laboratories, USA). The protein concentration was determined using protein assay DC (Bio-Rad, Hercules, USA). The protein lysate (50 μg and 200 μg) was separated with gel electrophoresis together with PageRuler prestained protein ladder (Fermentas, Canada) on a Mini-Protean TGX Precast gel (4–15%, Bio-Rad, Hercules, USA) in running buffer (0.1% SDS, 0.025 Tris base and 0.192 M glycine). The proteins were transferred to a Immobilon-P polyvinylidine fluoride (PVDF) membrane (Millipore, Billerica, USA) in transfer buffer (0.025 Tris base, 0.192 M glycine and 20% methanol) and pre-blocked for 1 h in blocking buffer (5% non-fat dry milk (Bio-Rad, Hercules, USA) diluted in 1.5 M NaCl, 0.1 M Tris, 0.05% Tween-20, pH 8.0). The membrane was hybridized with the diluted primary rabbit-anti-PAT4 (1:50, Sigma Aldrich, Sweden) overnight at 4 °C. The membrane was washed with TBST four times (1 × 1 min and 3 × 10 min) and incubated for 1 h with horseradish peroxidase conjugated goat anti-rabbit secondary antibody (diluted 1:10,000, Invitrogen, USA). This was followed by detection with the enhanced chemiluminescent (ECL) method and subsequent washes with TBST as previously described. The membrane was incubated for 3 min in a 1:1 mixture of luminol/enhancer and peroxidase buffer solution (Immun-Star HRP, Bio-Rad, USA) and developed on High performance chemiluminescence film (GE healthcare, USA).

4.9. *RNA-probe synthesis*

Mouse Slc36a4 EST clone ID IRCLp5011G0824D was used to synthesize the antisense probe. Plasmid cDNA was prepared with the JETstar 2.0 Plasmid Purification Mini Kit/50 (Genomed, Germany), the concentration was measured using a NanoDrop ND-1000 spectrophotometer (NanoDrop Technologies), and the clone was sequenced (Eurofins MWG Operon, Germany) and verified correct. The plasmid was cut with PstI (Fermentas, Latvia), and the probe was synthesized using 1 μg of cleaved vector as template with SP6 RNA polymerase in the presence of digoxigenin-11-UTP (Roche Diagnostics Scandinavia, Sweden). The digoxigenin-labeled mouse Slc36a4 probe was then quantified and controlled for integrity using the Experion RNA StdSens Analysis kit on an Experion automated electrophoresis system (Bio-Rad) and stored at −80 °C.

4.10. *Phylogenetic analysis*

The complete protein sequence datasets nine different genomes were mined using a Hidden Markov Model (HMM) trained on the human SLC36 family sequences. The sequences were filtered against a complete set of human SLC sequences, to remove false positive hits. The sequences were aligned using the E-INS_I version of MAFFT (Katoh et al., 2002) The alignment was manually edited and trimmed using Jalview (v. 2.6.1) (Waterhouse et al., 2009) to contain only the transmembrane regions. Incomplete sequences were removed. Thereafter, a phylogenetic tree was constructed using the Bayesian approach as implemented in MrBayes (Huelsenbeck and Ronquist, 2001; Ronquist and Huelsenbeck, 2003). The posterior probabilities were approximated using Markov Chain Monte Carlo (MCMC) analysis with a model allowing rate variation across sites under the invariate gamma distribution. The mixed amino acid model was used to estimate the optimal evolutionary model. The analysis was set to run for 5,000,000 generations and a stop rule was used

to terminate the analysis when the split frequencies were <0.01 and 1% of the trees were sampled. The first 25% of the trees were discarded and the remaining 75% of the trees were used to calculate a 50% majority rule consensus tree. The phylogenetic tree was drawn in TreeView (p. 1999) as an unrooted tree and edited in Canvas 12.

REFERENCES

Abbot, E.L., Grenade, D.S., Kennedy, D.J., Gatfield, K.M., Thwaites, D.T., 2006. Vigabatrin transport across the human intestinal epithelial (Caco-2) brush-border membrane is via the H+-coupled amino-acid transporter hPAT1. Br. J. Pharmacol. 147, 298–306.

Anderson, C.M., Grenade, D.S., Boll, M., Foltz, M., Wake, K.A., Kennedy, D.J., Munck, L.K., Miyauchi, S., Taylor, P.M., Campbell, F.C., Munck, B.G., Daniel, H., Ganapathy, V., Thwaites, D.T., 2004. H+/amino acid transporter 1 (PAT1) is the imino acid carrier: an intestinal nutrient/drug transporter in human and rat. Gastroenterology 127, 1410–1422.

Bermingham Jr., J.R., Shumas, S., Whisenhunt, T., Sirkowski, E.E., O'Connell, S., Scherer, S.S., Rosenfeld, M.G., 2002. Identification of genes that are downregulated in the absence of the POU domain transcription factor pou3f1 (Oct-6, Tst-1, SCIP) in sciatic nerve. J. Neurosci. 22, 10217–10231.

Bermingham Jr., J.R., Pennington, J., 2004. Organization and expression of the SLC36 cluster of amino acid transporter genes. Mamm. Genome 15, 114–125.

Bernhardt, R., Matus, A., 1984. Light and electron microscopic studies of the distribution of microtubule-associated protein 2 in rat brain: a difference between dendritic and axonal cytoskeletons. J. Comp. Neurol. 226, 203–221.

Boll, M., Foltz, M., Rubio-Aliaga, I., Kottra, G., Daniel, H., 2002. Functional characterization of two novel mammalian electrogenic proton-dependent amino acid cotransporters. J. Biol. Chem. 277, 22966–22973.

Boll, M., Foltz, M., Anderson, C.M., Oechsler, C., Kottra, G., Thwaites, D.T., Daniel, H., 2003a. Substrate recognition by the mammalian proton-dependent amino acid transporter PAT1. Mol. Membr. Biol. 20, 261–269.

Boll, M., Foltz, M., Rubio-Aliaga, I., Daniel, H., 2003b. A cluster of proton/amino acid transporter genes in the human and mouse genomes. Genomics 82, 47–56.

Boll, M., Daniel, H., Gasnier, B., 2004. The SLC36 family: proton-coupled transporters for the absorption of selected amino acids from extracellular and intracellular proteolysis. Pflugers Arch. 447, 776–779.

Broer, S., Bailey, C.G., Kowalczuk, S., Ng, C., Vanslambrouck, J.M., Rodgers, H., Auray-Blais, C., Cavanaugh, J.A., Broer, A., Rasko, J.E., 2008. Iminoglycinuria and hyperglycinuria are discrete human phenotypes resulting from complex mutations in proline and glycine transporters. J. Clin. Invest. 118, 3881–3892.

Broer, S., Palacin, M., 2011. The role of amino acid transporters in inherited and acquired diseases. Biochem. J. 436, 193–211.

Chen, Z., Fei, Y.J., Anderson, C.M., Wake, K.A., Miyauchi, S., Huang, W., Thwaites, D.T., Ganapathy, V., 2003a. Structure, function and immunolocalization of a proton-coupled amino acid transporter (hPAT1) in the human intestinal cell line Caco-2. J. Physiol. 546, 349–361.

Chen, Z., Kennedy, D.J., Wake, K.A., Zhuang, L., Ganapathy, V., Thwaites, D.T., 2003b. Structure, tissue expression pattern, and function of the amino acid transporter rat PAT2. Biochem. Biophys. Res. Commun. 304, 747–754.

Doyle, K.P., Cekanaviciute, E., Mamer, L.E., Buckwalter, M.S., 2010. TGFbeta signaling in the brain increases with aging and signals to astrocytes and innate immune cells in the weeks after stroke. J. Neuroinflammation 7, 62.

Foltz, M., Boll, M., Raschka, L., Kottra, G., Daniel, H., 2004a. A novel bifunctionality: PAT1 and PAT2 mediate electrogenic proton/amino acid and electroneutral proton/fatty acid symport. FASEB J. 18, 1758–1760.

Foltz, M., Oechsler, C., Boll, M., Kottra, G., Daniel, H., 2004b. Substrate specificity and transport mode of the proton-dependent amino acid transporter mPAT2. Eur. J. Biochem. 271, 3340–3347.

Franklin, K.B.J., Paxinos, G, 2007. The Mouse Brain in Stereotaxic Coordinates. Elsevier, New York.

Fredriksson, R., Nordstrom, K.J., Stephansson, O., Hagglund, M.G., Schioth, H.B., 2008. The solute carrier (SLC) complement of the human genome: phylogenetic classification reveals four major families. FEBS Lett. 582, 3811–3816.

Gasnier, B., 2004. The SLC32 transporter, a key protein for the synaptic release of inhibitory amino acids. Pflugers Arch. 447, 756–759.

Geerlings, A., Nunez, E., Rodenstein, L., Lopez-Corcuera, B., Aragon, C., 2002. Glycine transporter isoforms show differential subcellular localization in PC12 cells. J. Neurochem. 82, 58–65.

Hamon, M., Bourgoin, S., Artaud, F., Glowinski, J., 1979. The role of intraneuronal 5-HT and of tryptophan hydroxylase activation in the control of 5-HT synthesis in rat brain slices incubated in K+-enriched medium. J. Neurochem. 33, 1031–1042.

Hediger, M.A., Romero, M.F., Peng, J.B., Rolfs, A., Takanaga, H., Bruford, E.A., 2004. The ABCs of solute carriers: physiological, pathological and therapeutic implications of human membrane transport proteinsIntroduction. Pflugers Arch. 447, 465–468.

Hediger, M.A., Clemencon, B., Burrier, R.E., Bruford, E.A., 2013. The ABCs of membrane transporters in health and disease (SLC series): introduction. Mol. Aspects Med. 34, 95–107.

Heublein, S., Kazi, S., Ogmundsdottir, M.H., Attwood, E.V., Kala, S., Boyd, C.A., Wilson, C., Goberdhan, D.C., 2010. Proton-assisted amino-acid transporters are conserved regulators of proliferation and amino-acid-dependent mTORC1 activation. Oncogene 29, 4068–4079.

Huelsenbeck, J.P., Ronquist, F., 2001. MRBAYES: Bayesian inference of phylogenetic trees. Bioinformatics 17, 754–755.

Johnson, J.L., Roberts, E., 1984. Proline, glutamate and glutamine metabolism in mouse brain synaptosomes. Brain Res. 323, 247–256.

Katoh, K., Misawa, K., Kuma, K., Miyata, T., 2002. MAFFT: a novel method for rapid multiple sequence alignment based on fast Fourier transform. Nucleic Acids Res. 30, 3059–3066.

Kaufman, D.L., Houser, C.R., Tobin, A.J., 1991. Two forms of the gamma-aminobutyric acid synthetic enzyme glutamate decarboxylase have distinct intraneuronal distributions and cofactor interactions. J. Neurochem. 56, 720–723.

Mackenzie, B., Erickson, J.D., 2004. Sodium-coupled neutral amino acid (system N/A) transporters of the SLC38 gene family. Pflugers Arch. 447, 784–795.

McIntire, S.L., Reimer, R.J., Schuske, K., Edwards, R.H., Jorgensen, E.M., 1997. Identification and characterization of the vesicular GABA transporter. Nature 389, 870–876.

Mullen, R.J., Buck, C.R., Smith, A.M., 1992. NeuN, a neuronal specific nuclear protein in vertebrates. Development 116, 201–211.

Nishimura, M., Naito, S., 2005. Tissue-specific mRNA expression profiles of human ATP-binding cassette and solute carrier transporter superfamilies. Drug Metab. Pharmacokinet. 20, 452–477.

Palacin, M., Estevez, R., Bertran, J., Zorzano, A., 1998. Molecular biology of mammalian plasma membrane amino acid transporters. Physiol. Rev. 78, 969–1054.

Pillai, S.M., Meredith, D., 2011. SLC36A4 (hPAT4) is a high affinity amino acid transporter when expressed in Xenopus laevis oocytes. J. Biol. Chem. 286, 2455–2460.
Reeves, S.A., Helman, L.J., Allison, A., Israel, M.A., 1989. Molecular cloning and primary structure of human glial fibrillary acidic protein. Proc. Natl. Acad. Sci. U.S.A. 86, 5178–5182.
Ronquist, F., Huelsenbeck, J.P., 2003. MrBayes 3: Bayesian phylogenetic inference under mixed models. Bioinformatics 19, 1572–1574.
Ross, H.J., Wright, E.M., 1984. Neutral amino acid transport by plasma membrane vesicles of the rabbit choroid plexus. Brain Res. 295, 155–160.
Rubio-Aliaga, I., Boll, M., Vogt Weisenhorn, D.M., Foltz, M., Kottra, G., Daniel, H., 2004. The proton/amino acid cotransporter PAT2 is expressed in neurons with a different subcellular localization than its paralog PAT1. J. Biol. Chem. 279, 2754–2760.
Sagne, C., El Mestikawy, S., Isambert, M.F., Hamon, M., Henry, J.P., Giros, B., Gasnier, B., 1997. Cloning of a functional vesicular GABA and glycine transporter by screening of genome databases. FEBS Lett. 417, 177–183.
Sagne, C., Agulhon, C., Ravassard, P., Darmon, M., Hamon, M., El Mestikawy, S., Gasnier, B., Giros, B., 2001. Identification and characterization of a lysosomal transporter for small neutral amino acids. Proc. Natl. Acad. Sci. U.S.A. 98, 7206–7211.
Saier Jr., M.H., 2000. A functional-phylogenetic classification system for transmembrane solute transporters. Microbiol. Mol. Biol. Rev. 64, 354–411.
Soontornmalai, A., Vlaming, M.L., Fritschy, J.M., 2006. Differential, strain-specific cellular and subcellular distribution of multidrug transporters in murine choroid plexus and blood–brain barrier. Neuroscience 138, 159–169.
Sreedharan, S., Stephansson, O., Schioth, H.B., Fredriksson, R., 2011. Long evolutionary conservation and considerable tissue specificity of several atypical solute carrier transporters. Gene 478, 11–18.
Su, Y.H., Frommer, W.B., Ludewig, U., 2004. Molecular and functional characterization of a family of amino acid transporters from Arabidopsis. Plant Physiol. 136, 3104–3113.
Sundberg, B.E., Waag, E., Jacobsson, J.A., Stephansson, O., Rumaks, J., Svirskis, S., Alsio, J., Roman, E., Ebendal, T., Klusa, V., Fredriksson, R., 2008. The evolutionary history and tissue mapping of amino acid transporters belonging to solute carrier families SLC32, SLC36, and SLC38. J. Mol. Neurosci. 35, 179–193.
Thwaites, D.T., Anderson, C.M., 2011. The SLC36 family of proton-coupled amino acid transporters and their potential role in drug transport. Br. J. Pharmacol. 164, 1802–1816.
von Overbeck, J., Stahli, C., Gudat, F., Carmann, H., Lautenschlager, C., Durmuller, U., Takacs, B., Miggiano, V., Staehelin, T., Heitz, P.U., 1985. Immunohistochemical characterization of an anti-epithelial monoclonal antibody (mAB lu-5). Virchows Arch. A: Pathol. Anat. Histopathol. 407, 1–12.
Waterhouse, A.M., Procter, J.B., Martin, D.M., Clamp, M., Barton, G. J., 2009. Jalview Version 2—a multiple sequence alignment editor and analysis workbench. Bioinformatics 25, 1189–1191.
Westergaard, N., Varming, T., Peng, L., Sonnewald, U., Hertz, L., Schousboe, A., 1993. Uptake, release, and metabolism of alanine in neurons and astrocytes in primary cultures. J. Neurosci. Res. 35, 540–545.
Wiedenmann, B., Franke, W.W., 1985. Identification and localization of synaptophysin, an integral membrane glycoprotein of Mr 38,000 characteristic of presynaptic vesicles. Cell 41, 1017–1028.
Wipf, D., Ludewig, U., Tegeder, M., Rentsch, D., Koch, W., Frommer, W.B., 2002. Conservation of amino acid transporters in fungi, plants and animals. Trends Biochem. Sci. 27, 139–147.
Wreden, C.C., Johnson, J., Tran, C., Seal, R.P., Copenhagen, D.R., Reimer, R.J., Edwards, R.H., 2003. The H+-coupled electrogenic lysosomal amino acid transporter LYAAT1 localizes to the axon and plasma membrane of hippocampal neurons. J. Neurosci. 23, 1265–1275.
Young, G.B., Jack, D.L., Smith, D.W., Saier Jr., M.H., 1999. The amino acid/auxin:proton symport permease family. Biochim. Biophys. Acta 1415, 306–322.